Science
AAAS

Electrically Controlled Nonlinear Generation of Light with Plasmonics

Wenshan Cai, *et al.*

Science **333**, 1720 (2011);
DOI: 10.1126/science.1207858

PSR J1719−1438 demonstrates that, during binary pulsar evolution, special circumstances can conspire that allow neutron-star stellar companions to be transformed into exotic planets unlike those liable to be found anywhere else in the universe. The chemical composition, pressure, and dimensions of the companion ensure that it will be crystallized (i.e., diamond).

References and Notes

1. J. W. T. Hessels *et al.*, *Science* **311**, 1901 (2006); 10.1126/science.1123430.
2. D. Bhattacharya, E. P. J. van den Heuvel, *Phys. Rep.* **203**, 1 (1991).
3. J. E. Grindlay, C. D. Bailyn, *Nature* **336**, 48 (1988).
4. E. P. J. van den Heuvel, P. T. J. Bonsema, *Astron. Astrophys.* **139**, L16 (1984).
5. V. M. Kaspi *et al.*, *Astrophys. J.* **543**, 321 (2000).
6. P. T. J. Bonsema, E. P. J. van den Heuvel, *Astron. Astrophys.* **146**, L3 (1985).
7. A. S. Fruchter, D. R. Stinebring, J. H. Taylor, *Nature* **333**, 237 (1988).
8. B. W. Stappers, M. Bailes, R. N. Manchester, J. S. Sandhu, M. Toscano, *Astrophys. J.* **499**, L183 (1998).
9. A. Wolszczan, D. A. Frail, *Nature* **355**, 145 (1992).
10. E. P. J. van den Heuvel, *Nature* **356**, 668 (1992).
11. F. A. Rasio, S. L. Shapiro, S. A. Teukolsky, *Astron. Astrophys. J.* **256**, L35 (1992).
12. B. M. S. Hansen, H.-Y. Shih, T. Currie, *Astrophys. J.* **691**, 382 (2009).
13. P. Podsiadlowski, in *Planets Around Pulsars*, vol. 36 of *Astronomical Society of the Pacific Conference Series*, J. A. Phillips, S. E. Thorsett, S. R. Kulkarni, Eds. (Astronomical Society of the Pacific, San Francisco, 1993), pp. 149–165.
14. M. J. Keith *et al.*, *Mon. Not. R. Astron. Soc.* **409**, 619 (2010).
15. R. T. Edwards, M. Bailes, W. van Straten, M. C. Britton, *Mon. Not. R. Astron. Soc.* **326**, 358 (2001).
16. B. A. Jacoby, A. Hotan, M. Bailes, S. Ord, S. R. Kulkarni, *Astrophys. J.* **629**, L113 (2005).
17. J. P. W. Verbiest *et al.*, *Astrophys. J.* **679**, 675 (2008).
18. P. B. Demorest, T. Pennucci, S. M. Ransom, M. S. E. Roberts, J. W. T. Hessels, *Nature* **467**, 1081 (2010).
19. B. Paczyński, *Annu. Rev. Astron. Astrophys.* **9**, 183 (1971).
20. J. Frank, A. R. King, D. J. Raine, *Accretion Power in Astrophysics* (Cambridge Univ. Press, Cambridge, 1985).
21. M. J. Keith *et al.*, *Mon. Not. R. Astron. Soc.* **414**, 1292 (2011).
22. F. Camilo, S. E. Thorsett, S. R. Kulkarni, *Astrophys. J.* **421**, L15 (1994).
23. M. Toscano *et al.*, *Mon. Not. R. Astron. Soc.* **307**, 925 (1999).
24. J. M. Cordes, T. J. W. Lazio, (2002); http://arxiv.org/abs/astroph/0207156.
25. B. W. Stappers, M. H. van Kerkwijk, B. Lane, S. R. Kulkarni, *Astrophys. J.* **510**, L45 (1999).
26. C. J. Deloye, L. Bildsten, *Astrophys. J.* **598**, 1217 (2003).
27. D. K. Galloway, D. Chakrabarty, E. H. Morgan, R. A. Remillard, *Astrophys. J.* **576**, L137 (2002).
28. A. M. Juett, D. Psaltis, D. Chakrabarty, *Astrophys. J.* **560**, L59 (2001).
29. D. Lai, A. Abrahams, S. Shapiro, *Astrophys. J.* **377**, 612 (1991).

Acknowledgments: The Parkes Observatory is part of the Australia Telescope, which is funded by the Commonwealth of Australia for operation as a National Facility managed by CSIRO. This project is supported by the ARC Programmes under grants DP0985270, DP1094370, and CE110001020. Access to the Lovell telescope is funded through a Science and Technologies Facilities Council rolling grant. Keck telescope time is made available through a special collaborative program between Swinburne Univ. of Technology and California Institute of Technology. We are grateful to J. Roy and Y. Gupta for early attempts to obtain a pulsar position with the Giant Metrewave Radio Telescope.

Supporting Online Material

www.sciencemag.org/cgi/content/full/333/6050/1717/DC1
Supporting Data S1 and S2

25 May 2011; accepted 3 August 2011
Published online 25 August 2011;
10.1126/science.1208890

Electrically Controlled Nonlinear Generation of Light with Plasmonics

Wenshan Cai, Alok P. Vasudev, Mark L. Brongersma*

Plasmonics provides a route to develop ultracompact optical devices on a chip by using extreme light concentration and the ability to perform simultaneous electrical and optical functions. These properties also make plasmonics an ideal candidate for dynamically controlling nonlinear optical interactions at the nanoscale. We demonstrate electrically tunable harmonic generation of light from a plasmonic nanocavity filled with a nonlinear medium. The metals that define the cavity also serve as electrodes that can generate high direct current electric fields across the nonlinear material. A fundamental wave at 1.56 micrometers was frequency doubled and modulated in intensity by applying a moderate external voltage to the electrodes, yielding a voltage-dependent nonlinear generation with a normalized magnitude of ~7% per volt.

Plasmonics is able to process optical information beyond the conventional diffraction limit (*1*–*3*). The linear regime of plasmonic optics has been investigated considerably, with basic components such as waveguides (*4*–*6*), antennas (*7*, *8*), and interferometers (*9*, *10*) being realized. Conversely, nonlinear optical phenomena associated with plasmonics, in which the dielectric polarization in a metal-dielectric nanostructure responds to the local electric field in a high-order manner, remains relatively unexplored compared with their linear counterparts (*11*). Plasmonics facilitates dramatic enhancements of localized field intensities via metallic nanostructures, and a majority of nonlinear interactions scale with the local intensity of the optical field. Rather than relying on bulk crystals as necessitated by conventional nonlinear optics, plasmonics offers us the opportunity to manipulate nonlinear optical responses in sub-diffraction-limited volumes and the possibility to ease strict phase-matching conditions. Enhanced second-harmonic generation (SHG) of light has been observed in a variety of patterned metal films, including individual nanoapertures (*12*, *13*), periodic hole arrays (*14*, *15*), and metamaterial monolayers (*16*), as well as more complicated metal-dielectric systems combining metallic components and conventional nonlinear dielectrics (*17*–*19*). Wave mixing and frequency conversion of higher orders in plasmonic structures have also been explored (*20*–*24*).

Although the aforementioned results reveal the potential of engineered metallic structures to enhance various nonlinear optical interactions, all of these demonstrations are electrically passive. Nonlinear optics at reduced dimensions has recently captured a growing interest, where optical signals are nonlinearly tailored by themselves or a pump light (*25*, *26*). For a wide variety of photonic applications, including signal and information processing, it is desirable to electrically manipulate nonlinear processes such as harmonic generation. Immediately after the first demonstration of SHG, it was found that application of a dc electric field to the crystal calcite (*27*) induced a frequency doubling of light. This phenomenon was termed electric-field-induced second-harmonic (EFISH) generation. The SHG is attributed to a material's third-order nonlinear susceptibility $\chi^{(3)}(2\omega;\omega,\omega,0)$ rather than its second-order counterpart $\chi^{(2)}(2\omega;\omega,\omega)$, which drives conventional SHG.

The third-order nonlinear process involved in EFISH is typically very weak, and the original demonstration of this phenomenon in fact relied on large voltages (kilovolts), bulky optical crystals (millimeter-sized), and high-power lasers. In plasmonic-EFISH all of the above requirements are relaxed, and chip-scale integration of nanostructured devices can be realized. The nanoscale separation between the metallic parts in a plasmonic device implies that a modest voltage signal across the structure can induce a giant control field. The metallic nanocavity in conjunction with a plasmonic antenna can enhance localized light intensity by orders of magnitude. In our proposed plasmonic EFISH device (Fig. 1, A and B), a narrow slit serves as a nanoscale optical resonator for surface plasmon-polariton (SPP) waves and is surrounded by a grating-based optical antenna. The geometrical parameters for the structure were chosen to provide maximum light concentration. Because of the combined contributions of a Fabry-Pérot resonance of the SPPs supported by the nanoslit and the Bragg grating resonance associated with the periodic array of grooves, the electromagnetic energy density in the slit region is enhanced by about a factor of 80 with respect to that of the incident fundamental wave (ω) at a wavelength of 1.56 μm. The intensity buildup of the fundamental wave within the nanoslit yields a remarkable improvement of the

Geballe Laboratory for Advanced Materials, Stanford University, 476 Lomita Mall, Stanford, CA 94305, USA.

*To whom correspondence should be addressed. E-mail: brongersma@stanford.edu

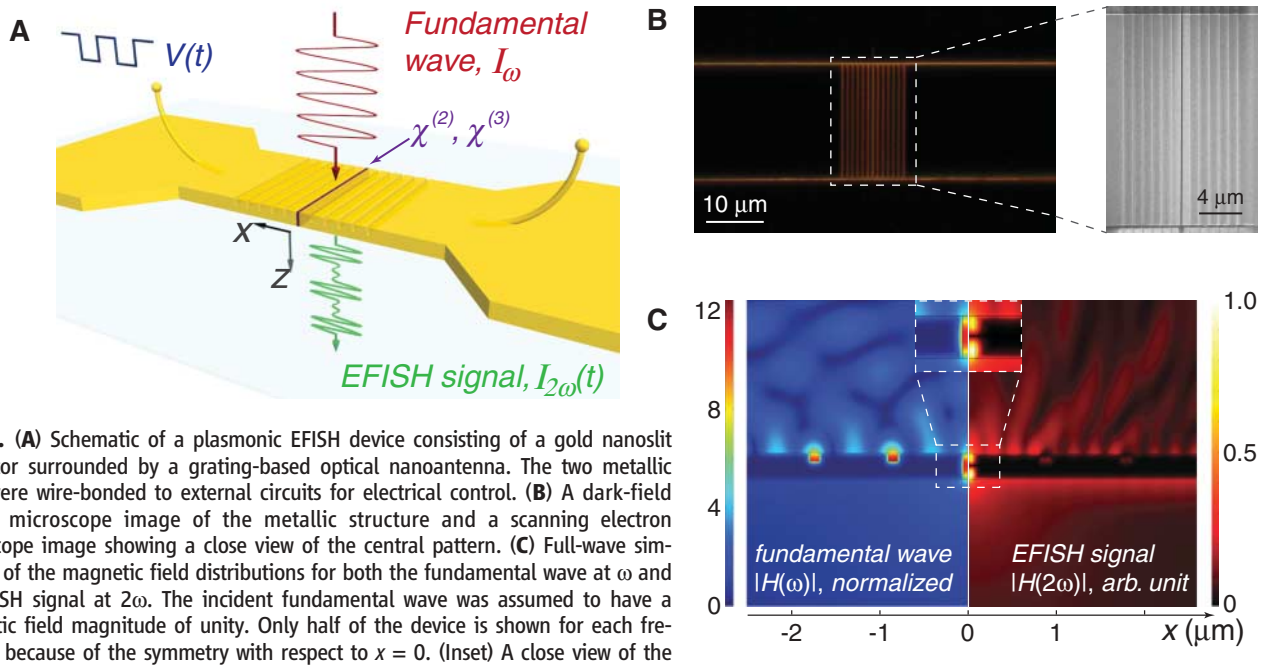

Fig. 1. (**A**) Schematic of a plasmonic EFISH device consisting of a gold nanoslit resonator surrounded by a grating-based optical nanoantenna. The two metallic parts were wire-bonded to external circuits for electrical control. (**B**) A dark-field optical microscope image of the metallic structure and a scanning electron microscope image showing a close view of the central pattern. (**C**) Full-wave simulation of the magnetic field distributions for both the fundamental wave at ω and the EFISH signal at 2ω. The incident fundamental wave was assumed to have a magnetic field magnitude of unity. Only half of the device is shown for each frequency because of the symmetry with respect to $x = 0$. (Inset) A close view of the plasmonic cavity.

SHG process, whose efficiency is proportional to the square of the local field intensity. The nanoslit, 100 nm wide, enables an intense electric field generated by a voltage magnitude compatible with standard chip-scale applications; a control voltage of 1 V produces an electric field strength E_c inside the nanoslit as high as 10^5 V/cm.

We placed a dielectric medium with both second- and third-order nonlinear susceptibilities into the metallic nanocavity. The frequency-doubled output contains not only a static component related to $\chi^{(2)}$ and the fundamental intensity but additional electrically tunable terms, which can be externally controlled by an applied voltage signal. Given that the electric field component of the plasmonic mode in the nanoslit is predominately transverse, we explain how SHG signals $I_{j,2\omega}$ polarized in the j direction can be generated with an x-polarized fundamental wave with an intensity $I_{x,\omega}$. The nonlinear polarization $P_{j,2\omega}$ and SHG intensity $I_{j,2\omega}$ can be expressed as

$$I_{j,2\omega} \propto |P_{j,2\omega}|^2 \propto |\chi^{(2)}_{jxx} + \chi^{(3)}_{jxxx}E_c|^2 I^2_{x,\omega}$$

The coordinates used in the discussion are shown in Fig. 1A, where x and z denote the directions of control field E_c and the light propagation direction, respectively. By expanding the right-hand side of the formula, we obtained a voltage-insensitive term $[\chi^{(2)}_{jxx}I_{x,\omega}]^2$ corresponding to conventional SHG, which will be subsequently referred to as the static SHG signal, as well as an extra voltage-controlled component $\Delta I_{j,2\omega}(E_c) \propto \{[\chi^{(3)}_{jxxx}E_c]^2 + 2\chi^{(2)}_{jxx}\chi^{(3)}_{jxxx}E_c\}I^2_{x,\omega}$. The dependence of the electrically induced nonlinear modulation $\Delta I_{j,2\omega}(E_c)$ on the control voltage V_c can be either quasi-linear or quadratic, depending on the comparative magnitudes of $\chi^{(2)}_{jxx}$ and $\chi^{(3)}_{jxxx}E_c$. To elucidate the linear and nonlinear properties of the designed device, we performed full-wave simulations for the plasmonic EFISH effect by using the finite element method (*28*). The field maps for both the fundamental wave at ω and the EFISH signal at 2ω are shown in Fig. 1C.

The experimental setup to detect the voltage-controlled SHG signal from our plasmonic-EFISH devices includes femtosecond laser pulses, polarization components, electric circuits, dispersive and filtering elements, imaging units, and lock-in systems (*28*). The nanocavity was filled with polymethyl methacrylate (PMMA). To prevent any undesired dielectric waveguide modes adjacent to the top metal surface, we subsequently coated the device with another thick layer of polyvinyl alcohol. The peak intensity of the fundamental beam (ω, 1.56 μm) is about 2.4×10^8 W/cm^2. The incident wave has its electric field polarized along the x direction, which is necessary for excitation of the plasmonic cavity resonance. To detect the SHG polarized in the x direction, we also placed a linear polarizer along the detection path.

The change in the SHG output from the plasmonic nanocavity as a function of an externally applied control voltage (Fig. 2) indicates a linear dependence of the frequency-doubled output on the control voltage, with the magnitude of the normalized change $\Delta I_{2\omega}(V_c)/I_{2\omega}(V_c = 0)$ being over 7% per volt. When a DC voltage of 20 V is applied across the nanocavity, the normalized tunability of the frequency-doubled output is 141%. A similar linear bias dependence is observed when we use an AC electrical pulse chain to drive the plasmonic EFISH device. The quasi-linear function $\Delta I_{2\omega}(V_c) \propto V_c$ implies that, between

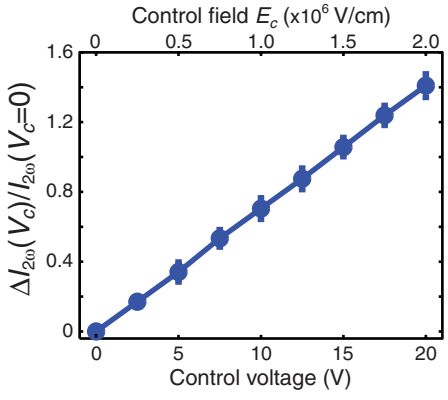

Fig. 2. The normalized change in the frequency-doubled output $\Delta I_{2\omega}$ as a function of externally applied voltage V_c. A nonlinear modulation magnitude of ~7% per volt and ~140% at a bias voltage of 20 V was observed. The data was collected with an output polarizer aligned along x direction. Error bars indicate standard deviations from five measurements. The magnitude of the control field E_c is shown on the upper axis.

the two electrically active terms in $\Delta I_{2\omega}(E_c)$, the cross term $\chi^{(2)}\chi^{(3)}E_c$ relying on both the second- and the third-order nonlinear susceptibilities dominates over the $[\chi^{(3)}E_c]^2$ term that relates to V_c in a quadratic manner.

The reasoning described above implies that the magnitude of the static SHG governed by $[\chi^{(2)}I_\omega]^2$ should surpass the EFISH signal, which, at a first glance, contradicts the nonlinear modulation of up to 141% observed in the experiment. The polarization states of different components of the total SHG output play an essential role in the magnitude of electrical tunability of the

plasmonic EFISH device. On the right axis of Fig. 3A we plot the electrically induced change in SHG without using the output polarizer in the experimental setup. Although the linear dependence of $\Delta I_{2\omega}(V_c) \propto V_c$ persists, the magnitude of the nonlinear modulation decreases by a factor of 6 as compared with the previous case when only the *x*-polarized signal is detected. We experimentally analyzed the polarization states of the static SHG and the voltage-controlled portion at $V_c = 10$ V (Fig. 3B). The EFISH signal is linearly polarized along the direction of the control field E_c, whereas the static SHG is predominately polarized normal to that with an extinction ratio of 5.3:1. This orthogonal relationship between the static and tunable parts of the frequency-doubled output gives us another degree of freedom to single out the voltage-controlled nonlinear generation.

Like the conventional SHG, the plasmonic EFISH signal $\Delta I_{2\omega}$ is expected to be quadratic with the intensity of the fundamental wave $I_{x,\omega}$ (Fig. 3C). We also measured the frequency-doubled signals while varying the polarization of the fundamental wave at a constant intensity (Fig. 3D). The angular lobe representing the polarization of the fundamental wave ω is substantially narrower than that of linearly polarized light because a $\cos^4\theta$ dependence is expected in this case, where θ denotes the direction of incident polarization with respect to the *x* axis. Spectrally or angularly, the second harmonic peak is narrower than the fundamental peak, reflecting the expected nonlinear intensity dependence.

A range of control measurements have been performed to rule out other possible sources of the collected data (*28*). We verified that there is no detectable emission at 2ω beyond the noise level originating from either the polymer-coated substrate or the unpatterned gold film. Illuminating the metallic nanodevice with *y*-polarized fundamental wave also does not provide detectable SHG signals, because the cavity resonance cannot be excited when the incident electric field of light is polarized along the nanoslit. We also tested the same metallic pattern without a polymer coating, and measured static SHG power emerging from the uncoated plasmonic structure is one order of magnitude lower than that of the polymer-coated device. In addition, there is absolutely no detectable variation of the SHG output when a voltage is applied to the uncoated sample. This reveals that the electrical activity of the plasmonic-EFISH device is derived from the polymer filler rather than the metallic nanostructure.

In the preceding discussion, we assumed the nonlinear behavior in the slit medium to exhibit bulk properties, that the PMMA polymer filled within the nano-gap is homogeneous, and that all nonlinear activity can be attributed to electric fields along the *x* direction. For simplicity, we have not explicitly included the nonlinear susceptibilities related to the surfaces. This assumption may deviate from the actuality for at least two reasons. First, the orientational distribution of the polymer confined within a nanocavity is not necessarily uniform. Second, the electric field of the plasmonic gap mode in the nanoslit contains also a *z*-component $E_{z,\omega}$ bound to the metal-polymer interface with a magnitude roughly five times less than $E_{x,\omega}$, along with local hotspots at the corners of the slit region. Other than the nonlinear susceptibilities associated with the polymer filling the slit, another possible contribution to the detected SHG signal is the effective $\chi^{(2)}$ arising from the broken symmetry at metallic boundaries. We have not estimated quantitatively how the experimental data compare to numerical simulations because the exact values for all pertinent

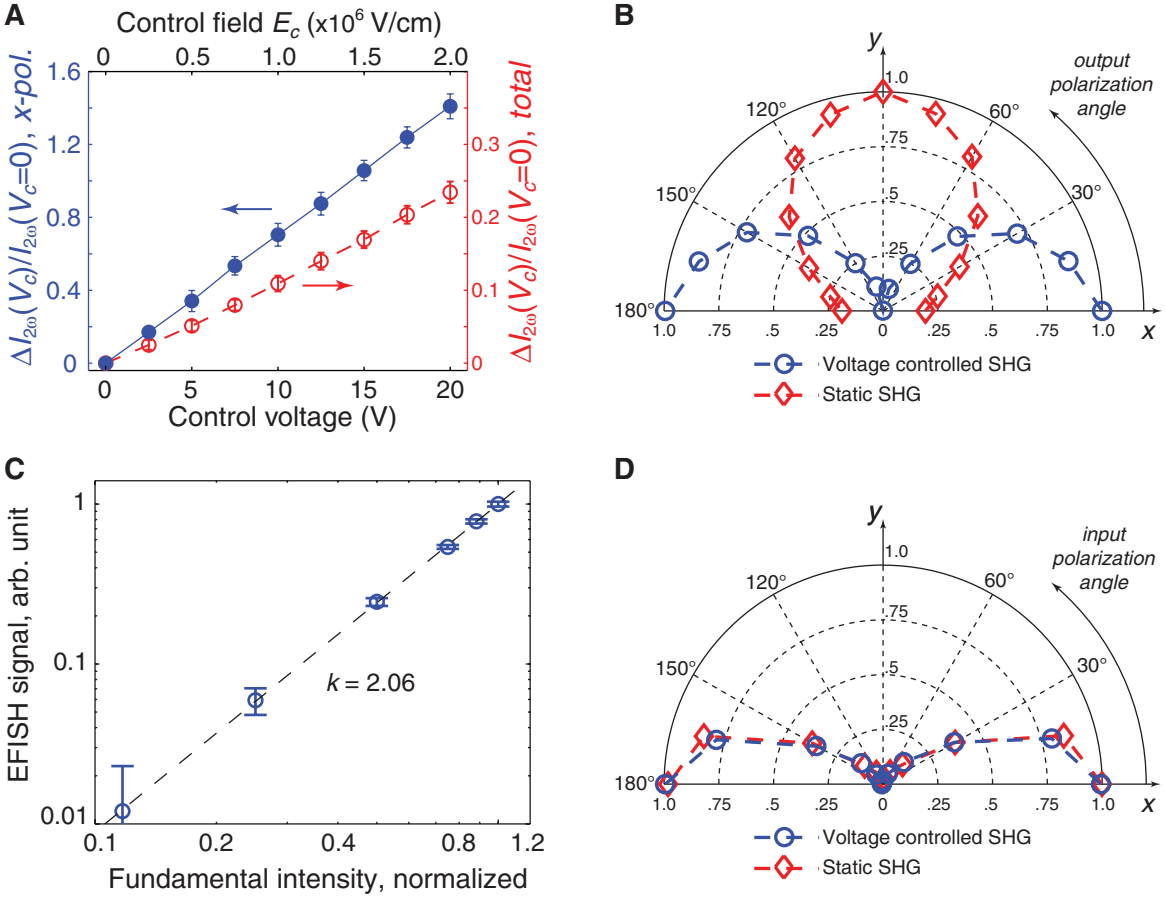

Fig. 3. (**A**) Double-Y plot showing the dependence of the normalized $\Delta I_{2\omega}$ signal on the applied voltage V_c. The blue markers and the left axis reproduce the data in Fig. 2, and the right axis corresponds to the same quantity without the implementation of the output polarizer. Error bars indicate standard deviations from five measurements. (**B**) Polar diagram showing the polarization property of the frequency-doubled output signal. The pump light, at a fixed intensity, was linearly polarized along the *x* axis. The diamond markers represent the state of polarization of the static SHG in the absence of applied voltage, and the open circles denote the polarization of the voltage-controlled EFISH signal at $V_c = 10$ V. Each curve is normalized to its respective maximum value. For symmetry reasons, only half of the 2π angular space is shown in the polar plot. (**C**) The voltage-controlled EFISH output $\Delta I_{2\omega}$ as a function of the intensity of the fundamental wave. Error bars represent standard deviations based on five measurements. The dashed line indicates a least-squares fit using the function $\Delta I_{2\omega}(I_\omega) \propto I_\omega^{\,k}$. The least-squares fit exponent was found to be $k = 2.06$. (**D**) The static SHG output $I_{2\omega}(V_c = 0)$ and its electrical modulation $\Delta I_{2\omega}$ at $V_c = 10$ V as functions of the polarization state of the fundamental wave of a constant intensity. No polarizer for the output signal was used in this measurement. The diamond and circular markers represent the static and EFISH signals, respectively.

elements of the nonlinear susceptibility tensors are not readily available. A consistent microscopic theory of the nonlinear response of polymers taking into account the molecular alignments and their electric activities is beyond the scope of this work. We conservatively estimate the efficiency of the plasmonic EFISH process to be 5.7×10^{-11} at $V_c = 20$ V. This value is on the same order magnitude as the conventional SHG conversion efficiency in a prototypical nonlinear crystal of the same thickness and under the same experimental conditions.

The plasmonic-EFISH devices demonstrated in this work can be generalized to other electrically controlled plasmonic frequency converters that are compact and relatively efficient and require no phase matching, rendering them suitable for chip-scale applications where integration is necessary.

References and Notes

1. R. Zia, J. A. Schuller, A. Chandran, M. L. Brongersma, *Mater. Today* **9**, 20 (2006).
2. H. A. Atwater, *Sci. Am.* **296**, 56 (2007).
3. M. L. Brongersma, V. M. Shalaev, *Science* **328**, 440 (2010).
4. R. Zia, M. D. Selker, P. B. Catrysse, M. L. Brongersma, *J. Opt. Soc. Am. A* **21**, 2442 (2004).
5. T. W. Ebbesen, C. Genet, S. I. Bozhevolnyi, *Phys. Today* **61**, 44 (2008).
6. W. S. Cai, W. Shin, S. H. Fan, M. L. Brongersma, *Adv. Mater.* **22**, 5120 (2010).
7. P. Mühlschlegel, H. J. Eisler, O. J. F. Martin, B. Hecht, D. W. Pohl, *Science* **308**, 1607 (2005).
8. E. S. Barnard, J. S. White, A. Chandran, M. L. Brongersma, *Opt. Express* **16**, 16529 (2008).
9. H. F. Schouten *et al.*, *Phys. Rev. Lett.* **94**, 053901 (2005).
10. R. Zia, M. L. Brongersma, *Nat. Nanotechnol.* **2**, 426 (2007).
11. J. A. Schuller *et al.*, *Nat. Mater.* **9**, 193 (2010).
12. A. Nahata, R. A. Linke, T. Ishi, K. Ohashi, *Opt. Lett.* **28**, 423 (2003).
13. P. Schön *et al.*, *Opt. Lett.* **35**, 4063 (2010).
14. M. Airola, Y. Liu, S. Blair, *J. Opt. A* **7**, S118 (2005).
15. J. A. H. van Nieuwstadt *et al.*, *Phys. Rev. Lett.* **97**, 146102 (2006).
16. M. W. Klein, C. Enkrich, M. Wegener, S. Linden, *Science* **313**, 502 (2006).
17. J. C. Quail, J. G. Rako, H. J. Simon, R. T. Deck, *Phys. Rev. Lett.* **50**, 1987 (1983).
18. W. Fan *et al.*, *Nano Lett.* **6**, 1027 (2006).
19. K. Chen, C. Durak, J. R. Heflin, H. D. Robinson, *Nano Lett.* **7**, 254 (2007).
20. S. Kim *et al.*, *Nature* **453**, 757 (2008).
21. M. Danckwerts, L. Novotny, *Phys. Rev. Lett.* **98**, 026104 (2007).
22. T. J. Xu, X. J. Jiao, S. Blair, *Opt. Express* **17**, 23582 (2009).
23. H. Harutyunyan, S. Palomba, J. Renger, R. Quidant, L. Novotny, *Nano Lett.* **10**, 5076 (2010).
24. P. Genevet *et al.*, *Nano Lett.* **10**, 4880 (2010).
25. J. Leuthold, C. Koos, W. Freude, *Nat. Photonics* **4**, 535 (2010).
26. M. A. Foster *et al.*, *Nature* **441**, 960 (2006).
27. R. W. Terhune, P. D. Maker, C. M. Savage, *Phys. Rev. Lett.* **8**, 404 (1962).
28. Materials and methods are available as supporting material on *Science* Online.

Acknowledgments: We acknowledge funding from the Air Force Office of Scientific Research (G. Pomrenke; STTR Phase I grant no. FA9550-10-C-0007 and grant no. FA9550-10-1-0264). We also gratefully acknowledge F. Afshinmanesh, E. S. Barnard, Y. C. Jun, and D. Kong for their assistance during various phases of the experiment.

Supporting Online Material

www.sciencemag.org/cgi/content/full/333/6050/1720/DC1
Materials and Methods
SOM Text
Figs. S1 to S4
References (*29*–*47*)

3 May 2011; accepted 8 August 2011
10.1126/science.1207858

Coherent Two-Dimensional Nanoscopy

Martin Aeschlimann,[1] Tobias Brixner,[2,3]* Alexander Fischer,[1] Christian Kramer,[2] Pascal Melchior,[1] Walter Pfeiffer,[4] Christian Schneider,[1] Christian Strüber,[4] Philip Tuchscherer,[2] Dmitri V. Voronine[4]†

We introduce a spectroscopic method that determines nonlinear quantum mechanical response functions beyond the optical diffraction limit and allows direct imaging of nanoscale coherence. In established coherent two-dimensional (2D) spectroscopy, four-wave–mixing responses are measured using three ingoing waves and one outgoing wave; thus, the method is diffraction-limited in spatial resolution. In coherent 2D nanoscopy, we use four ingoing waves and detect the final state via photoemission electron microscopy, which has 50-nanometer spatial resolution. We recorded local nanospectra from a corrugated silver surface and observed subwavelength 2D line shape variations. Plasmonic phase coherence of localized excitations persisted for about 100 femtoseconds and exhibited coherent beats. The observations are best explained by a model in which coupled oscillators lead to Fano-like resonances in the hybridized dark- and bright-mode response.

In all implementations of optical spectroscopy, the spatial interaction volume has a lower bound determined by the diffraction limit of light. The laser focus diameter is always larger than roughly half the optical excitation wavelength, and measurements represent averages over a distribution of quantum systems present within the interaction volume. Single-emitter experiments are possible when only one quantum system contributes to the measurement signal through a combination of tight focusing and low emitter density. This method avoids ensemble averaging, and although ultrafast femtosecond experiments have recently been realized (*1*, *2*), the spatial resolution is still diffraction-limited. Subdiffraction imaging resolution can be obtained via reversible fluorophore saturation such that only one emitter is active within the focal spot (*3*). This method works well for imaging but makes ultrafast spectroscopy challenging because the transitions need to be saturated. Near-field methods provide another way to achieve subdiffraction resolution (*4*), and ultrafast experiments have been performed (*5*). For these methods, one needs to implement raster scanning of the sample to obtain spatial-spectral information sequentially for each spot, and near-field two-dimensional (2D) spectroscopy has not yet been reported.

Here, we introduce coherent two-dimensional nanoscopy, which we define as the measurement of optical response functions using 2D spectroscopy with a spatial resolution below the optical diffraction limit. In contrast to potential near-field implementations, our technique uses wide-field illumination and detects 2D spectral information simultaneously for ~10^6 different spatial locations. In conventional 2D spectroscopy (*6*–*9*), the "input" to a four-wave mixing scheme consists of three incident waves that create a transient coherence (i.e., third-order polarization), which is then radiated off as the "output." However, coherent detection is not necessarily required; fluorescence (*10*, *11*) or electrons (*12*) can also be used. In coherent 2D nanoscopy, all four waves are input fields, and the output corresponds to excited electrons. The key

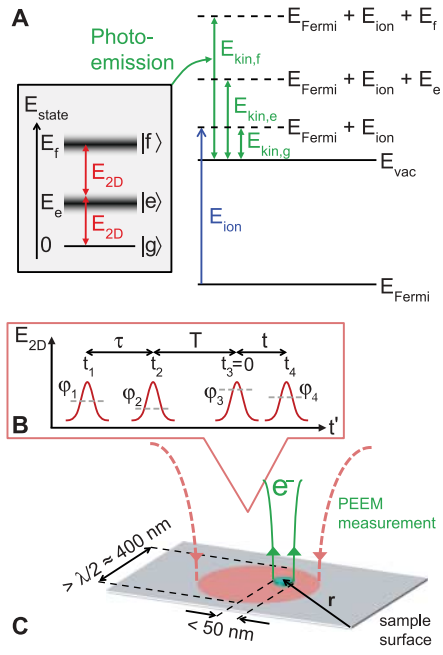

Fig. 1. Principle of coherent 2D nanoscopy. (**A**) Excitation of a quantum three-level system (left) leads to emission of photoelectrons with different kinetic energies (right). (**B**) A sequence of four femtosecond laser pulses is used for excitation. (**C**) The optical spot on the sample is larger than half the optical excitation wavelength (i.e., the diffraction limit), but photoemission electron microscopy (PEEM) provides 50-nm spatial resolution.

[1]Fachbereich Physik and Research Center OPTIMAS, Technische Universität Kaiserslautern, Erwin-Schrödinger-Str. 46, 67663 Kaiserslautern, Germany. [2]Institut für Physikalische und Theoretische Chemie, Universität Würzburg, Am Hubland, 97074 Würzburg, Germany. [3]Röntgen Research Center for Complex Material Systems, Am Hubland, 97074 Würzburg, Germany. [4]Fakultät für Physik, Universität Bielefeld, Universitätsstr. 25, 33615 Bielefeld, Germany.

*To whom correspondence should be addressed. E-mail: brixner@phys-chemie.uni-wuerzburg.de
†Present address: Institute for Quantum Science and Engineering, Texas A&M University, College Station, TX 77840, USA.